

Predicting Closed-Loop Performance of Latent World Models: Offline Checkpoint Selection for MPC and Model-Based RL Under Non-Markovian Rewards in LunarLander

Nikolai Smolyanskiy*

Abstract

We study how to predict the downstream closed-loop performance of a learned latent world model from validation-time diagnostics alone. Choosing the right checkpoint from a world-model training run is difficult: validation loss and multi-step prediction RMSE keep improving long after closed-loop performance has collapsed. We present a suite of structural validation-time diagnostics drawn from optimal-control theory and apply them to Gymnasium’s LunarLander-v3, which features shaped rewards. We train an RSSM [5, 4] world model on it and treat per-checkpoint CEM-MPC return as the oracle for closed-loop quality. By evaluating 40 metrics against this oracle, we find that the strongest single predictor is the Reward Observability Fraction (ROF), which measures the reward predictor’s dependence on the observable subspace. We combine ROF with three structural regularizers into a single-number offline checkpoint-selection score, the Composite Reward Observability Fraction (CROF). The CROF-selected world model trains a model-based A2C policy that beats a fairly evaluated model-free A2C baseline by ~ 24.5 return points while using $\sim 65\times$ fewer real-environment interactions, and the same world model also drives a strong zero-shot CEM-MPC policy. Code and data: https://github.com/nsmoly/LunarLander_RSSM.

1 Introduction

Model-based reinforcement learning promises to reduce the number of real-environment interactions needed to learn effective policies by building a predictive model of the environment—a *world model*—and using it for planning or policy optimization in imagination. The Dreamer or Recurrent State Space Model (RSSM) architecture [5, 4] has become a standard backbone for world models, enabling both online planning via Model Predictive Control (MPC) [5] and policy learning with Reinforcement Learning (RL) through imagined rollouts [4, 6].

A fundamental challenge in model-based RL is *objective mismatch* [8]: the training objective for the world model (prediction accuracy) does not necessarily align with the downstream objective (closed-loop performance). A model with excellent one-step or even multi-step prediction accuracy may still be unsuitable for planning or policy optimization if its learned latent dynamics lack the structural properties needed for these purposes.

In this work, we focus on the LunarLander-v3 Gymnasium environment. It has not been the subject of detailed RSSM/Dreamer-style analysis in prior work and combines two useful properties: an 8-dimensional observation and 4 discrete actions, both small enough to admit direct structural analysis of the learned latent, and—the property that motivates this paper—a reward that is not

*Code and experimental data: https://github.com/nsmoly/LunarLander_RSSM.

Video: https://youtu.be/4PxHFW_TYUw.

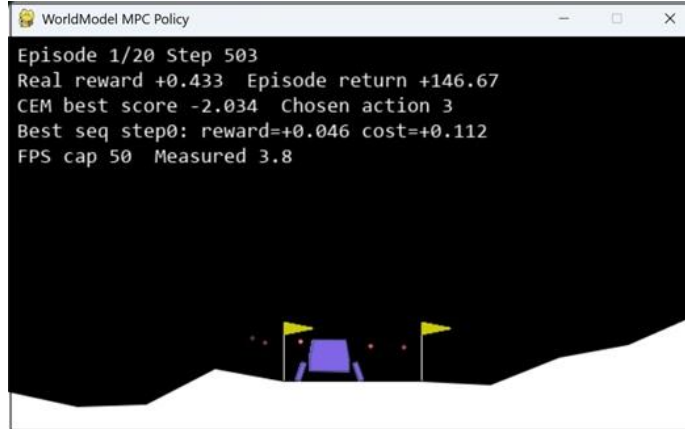


Figure 1: LunarLander-v3: four discrete actions (NOP, left/main/right thruster), 8-D observation, soft-landing objective from a randomized initial state.

fully recoverable from the current observation and action alone because of potential-based shaping plus terminal events gated by simulator-internal flags (Section 4.8). LunarLander thus serves as a tractable proxy for the broader class of environments with non-Markovian or shaped reward, where standard one-step prediction metrics turn out to be poor checkpoint-selection criteria. We develop structural diagnostics drawing on classical control theory (controllability, observability, Kalman [7]) and show experimentally that they identify world-model checkpoints that produce substantially better downstream policies than standard model-selection criteria, both for MPC and for model-based actor-critic policy trained in imagination.

Our contributions in this work are:

1. A suite of 40 structural validation-time metrics for world-model evaluation, drawing on classical control theory: Jacobian-based controllability/observability analysis (fixed and time-varying linearizations) and three reward/observation subspace-alignment scores.
2. The Composite Reward Observability Fraction (CROF), a single-number offline checkpoint-selection score that combines reward/observation subspace-alignment score with three structural scores (controllability rank, observability rank, open-loop observation error).
3. Experimental evidence on LunarLander-v3 that CROF tracks both zero-shot CEM-MPC returns and downstream A2C training quality, enabling offline selection of better world-model checkpoints for closed-loop use, while standard selection criteria (validation loss, multi-step RMSE, sensitivities) pick overfit checkpoints with poor closed-loop performance.
4. A data-efficiency comparison showing that the CROF-selected world model trains a model-based A2C policy that beats a fairly evaluated model-free A2C baseline using $\sim 65\times$ fewer real-environment interactions.

2 Related Work

Our work draws on three areas: world models for control, the objective mismatch problem in model-based RL, and classical control-theoretic analysis of dynamical systems.

2.1 World Models and Model-Based RL

The RSSM family — PlaNet [5], Dreamer [4], and DreamerV3 [6] — learns latent dynamics for planning and imagination-based actor-critic training; PETS [2] pairs probabilistic ensemble dynamics with MPC for strong sample efficiency. All of these methods train by maximizing prediction likelihood and evaluate by downstream task performance, without analyzing the structural properties of the learned dynamics that determine planning quality.

2.2 Objective Mismatch

Lambert et al. [8] identified the *objective mismatch* problem: optimizing a dynamics model for one-step prediction accuracy does not guarantee good downstream closed-loop performance, and proposed re-weighting training objectives as an initial mitigation. Our work proposes a complementary explanation of why this mismatch occurs: prediction accuracy (even multi-step) captures statistical fit, while planning quality depends on the structural alignment between reward-relevant, controllable, and observable subspaces — a geometric property that training losses do not measure.

2.3 Task-Relevant Representations

Several works learn representations that preserve task-relevant information at training time: DeepMDP [3] via bisimulation-inspired losses on reward and transition structure, SOLAR [14] by encouraging locally linear dynamics for LQR planning from images, and Agarwal et al. [1] via contrastive embeddings of behavioral similarity. These approaches modify the training objective. Our work is complementary: we provide post-hoc validation-time diagnostics that quantify whether the learned structure supports closed-loop planning, regardless of training procedure.

2.4 Control-Theoretic Analysis of Learned Systems

Controllability and observability originate with Kalman [7], who showed that the rank of the corresponding matrices determines whether a linear system can be fully steered and observed; Moore [9] extended this with balanced realization theory, identifying dimensions that are simultaneously controllable and observable. Sussillo and Barak [13] applied local Jacobian and fixed-point analysis to trained RNNs in neuroscience, revealing interpretable low-dimensional dynamics in high-dimensional recurrent networks. We adapt these tools to the RSSM setting and combine them into scalar reward/observation alignment fractions (RCF, OCF, ROF) used as post-hoc validation-time diagnostics that predict closed-loop performance without environment access.

3 Method

3.1 World Model Architecture

We use an RSSM-inspired world model [4, 6] adapted for LunarLander-v3, whose observation is $p=8$ -dimensional (6 continuous physics dimensions plus 2 binary leg-contact indicators) with $K=4$ discrete actions. The RSSM core maintains a deterministic hidden state $\mathbf{h}_t \in \mathbb{R}^{d_h}$ ($d_h=256$, single-layer GRU) and a stochastic latent $\mathbf{z}_t \in \mathbb{R}^{d_z}$ ($d_z=16$), giving a full latent state $\mathbf{s}_t = [\mathbf{h}_t; \mathbf{z}_t] \in \mathbb{R}^{272}$. Actions $a_t \in \{0, 1, 2, 3\}$ are one-hot encoded as $\mathbf{u}_t \in \mathbb{R}^4$. The RSSM transition (prior) is

$$\mathbf{s}_{t+1} = f_\theta(\mathbf{s}_t, \mathbf{u}_t) = [\text{GRU}(\mathbf{h}_t, [\mathbf{z}_t; \mathbf{u}_t]); \boldsymbol{\mu}_{\text{prior}}(\mathbf{h}_{t+1})], \quad (1)$$

the posterior encoder is $q_\theta(\mathbf{z}_t \mid \mathbf{h}_t, \mathbf{o}_t)$, and both prior and posterior are 2-layer MLPs (LayerNorm + SiLU) predicting mean and log-std of a diagonal Gaussian; the observation encoder is a 2-layer MLP mapping $\mathbf{o}_t \in \mathbb{R}^8$ to a feature vector concatenated with \mathbf{h}_t for the posterior.

Structured decoder with heterogeneous heads. Rather than treating all 8 observation dimensions identically, the decoder uses a shared 2-layer MLP backbone (LayerNorm + SiLU, input $d_h+d_z=272$) feeding four heads: an MSE-regression *physics* head (\mathbb{R}^6 , continuous states), a BCE *contact* head (\mathbb{R}^2 logits, sigmoid at inference), a BCE *done* head (\mathbb{R}^1), and a separate 3-layer *reward* MLP ($\mathbb{R}^{272} \rightarrow 256 \rightarrow 256 \rightarrow 1$) that operates directly on $[\mathbf{h}; \mathbf{z}]$ rather than the shared backbone, so the reward predictor develops its own representation without competing with reconstruction for backbone capacity. The observation decoder is $\hat{\mathbf{o}}_t = g_\theta(\mathbf{s}_t)$ (physics concatenated with sigmoid of contact logits); the reward predictor is $\hat{r}_t = \rho_\theta(\mathbf{s}_t)$.

Training loss. The total loss is a weighted sum:

$$\mathcal{L} = w_r \mathcal{L}_{\text{recon}} + w_\rho \mathcal{L}_{\text{rew}} + w_d \mathcal{L}_{\text{done}} + w_{\text{KL}} \mathcal{L}_{\text{KL}}, \quad (2)$$

with weights $w_r=1.0$, $w_\rho=1.2$, $w_d=0.5$, $w_{\text{KL}}=1.0$ (KL free-bits floor $\beta_{\text{KL}}=0.5$). $\mathcal{L}_{\text{recon}}$ combines MSE for physics and BCE for contacts; \mathcal{L}_{rew} is squared reward error; $\mathcal{L}_{\text{done}}$ is done-flag BCE; $\mathcal{L}_{\text{KL}} = \text{KL}(q_\theta \| p_\theta)$ is the posterior–prior KL divergence.

3.2 MPC via Cross-Entropy Method (CEM)

Since LunarLander-v3 has a discrete action space (4 actions: NOP, left thruster, main engine, right thruster), standard gradient-based planning does not apply. We use the Cross-Entropy Method (CEM) [11] adapted for discrete actions: at each real timestep, CEM iteratively refines a per-step categorical distribution over a planning horizon of $H=25$ steps. Each iteration samples $N=384$ candidate action sequences from the current distribution, rolls each one through the world-model prior open-loop while accumulating discounted reward $\sum_{k=1}^H \gamma^{k-1} \hat{r}_{t+k}$ ($\gamma=0.97$), keeps the top $E=48$ elites, and updates the per-step logits toward the elite action frequencies with smoothing factor $\alpha=0.7$. After $I=4$ such iterations, the first action of the best sequence is executed and the procedure repeats at the next real timestep. The planning horizon $H=25$ matches the rollout horizon used for metric evaluation, so the offline metrics measure exactly the regime CEM operates in.

3.3 Actor-Critic Policy via Latent Imagination

Following Dreamer [4], we train an actor–critic policy (A2C) entirely within the latent imagination of the world model. The actor and critic are compact 3-layer MLPs (hidden dimension of 256) that read the latent state $[\mathbf{h}; \mathbf{z}]$; the actor outputs a categorical distribution over the 4 actions, the critic predicts scalar value estimates. Each training step samples a real observation–action sequence from the replay dataset, warms the RSSM posterior up for 5 steps on the real data, then imagines 15 further steps by rolling out the prior with actions sampled from the actor (no observation correction). Value targets are λ -returns [12] ($\gamma=0.99$, $\lambda=0.95$) computed from the world model’s reward head; the actor is updated by REINFORCE with advantage clipping, the critic by MSE, and entropy is decayed from 0.5 to 0.15 over training. We train for 1000 epochs at learning rate 3×10^{-5} and batch size 256. Crucially, this stage uses *zero additional real-environment interactions*: all learning happens in the learned world model on the same offline dataset used to train it.

3.4 Metrics for World Model Quality

We define metrics in four categories; the full per-metric list with empirical correlations against MPC return is consolidated in Table 1 of Section 4.5.

3.4.1 Validation Loss Decomposition

Five standard training diagnostics: `val_loss` (total weighted validation loss as in (2)), its components `val_kl` (posterior–prior KL) and `val_recon` (physics + contact reconstruction), and the one-step posterior RMSEs `post_obs_rmse` and `post_rew_rmse`, which measure closed-loop prediction quality with encoder corrections.

3.4.2 Multi-Step Open-Loop Rollout

These metrics measure what CEM MPC experiences during planning: multi-step prediction quality without encoder corrections. After a 5-step posterior warm-up, the RSSM prior is rolled out for 25 steps using ground-truth actions, with squared errors masked over valid (non-padded, pre-terminal) positions and reduced by a square root. We record nine quantities: observation RMSE at the first horizon step (`ol_obs_start`), averaged across the horizon (`ol_obs_avg`), the per-rollout maximum (`ol_obs_max`), and at the last step (`ol_obs_end`); the same four for reward (`ol_rew_start`, `ol_rew_avg`, `ol_rew_max`, `ol_rew_end`); and the cumulative-reward RMSE `ol_cumrew_err` of $\sum_{k=1}^H \hat{r}_{t+k}$ against ground truth.

3.4.3 Jacobian-Based Linear Analysis

We linearize the transition, decoder, and reward functions around sampled validation states and apply classical control-theoretic analysis [7].

At a state $\mathbf{s} = [\mathbf{h}; \mathbf{z}]$ with action \mathbf{u} , the Jacobians are:

$$A = \left. \frac{\partial f_\theta}{\partial \mathbf{s}} \right|_{\mathbf{s}, \mathbf{u}} \in \mathbb{R}^{n \times n}, \quad B = \left. \frac{\partial f_\theta}{\partial \mathbf{u}} \right|_{\mathbf{s}, \mathbf{u}} \in \mathbb{R}^{n \times K}, \quad (3)$$

$$C = \left. \frac{\partial g_\theta}{\partial \mathbf{s}} \right|_{\mathbf{s}} \in \mathbb{R}^{p \times n}, \quad R = \left. \frac{\partial \rho_\theta}{\partial \mathbf{s}} \right|_{\mathbf{s}} \in \mathbb{R}^{1 \times n}. \quad (4)$$

Fixed vs. time-varying linearization. In *fixed* linearization (`jac_` prefix), Jacobians A, B, C, R are computed once at a sampled state and the controllability/observability matrices use powers A^k : $\mathcal{C}_H = [B, AB, \dots, A^{H-1}B]$, $\mathcal{O}_H = [C; CA; \dots; CA^{H-1}]$. In *time-varying* linearization (`jac_dyn_` prefix), fresh Jacobians A_k, B_k, C_k, R_k are computed at each step of an actual latent rollout through the prior and the matrices chain along that rollout. Every Jacobian metric below is computed in both variants; Section 4.6 compares them empirically.

Spectral and rank summaries. From A and from $\mathcal{C}_H, \mathcal{O}_H$ we record six scalar summaries: the mean spectral radius of A (`jac_spec_radius`) and its per-sample maximum (`jac_spec_radius_max`); the effective controllability rank k_c (`jac_ctrl_rank`) and its singular-value condition number $\sigma_1(\mathcal{C}_H)/\sigma_{k_c}(\mathcal{C}_H)$ (`jac_ctrl_cond`); and the analogous `jac_obs_rank` and `jac_obs_cond` for \mathcal{O}_H . Effective ranks use a threshold of 10^{-3} relative to the largest singular value. The same six are recorded with the `jac_dyn_` prefix for time-varying linearization (`jac_dyn_spec_radius`, `jac_dyn_spec_radius_max`, `jac_dyn_ctrl_rank`, `jac_dyn_ctrl_cond`, `jac_dyn_obs_rank`, `jac_dyn_obs_cond`).

Subspace alignment metrics. SVD the controllability and observability matrices as $\mathcal{C}_H = U_c \Sigma_c V_c^\top$ and $\mathcal{O}_H = U_o \Sigma_o V_o^\top$. Let $U_c^{(k)} \in \mathbb{R}^{n \times k_c}$ and $V_o^{(k)} \in \mathbb{R}^{n \times k_o}$ be the controllable and observable subspace bases, $\mathbf{r} = R^\top \in \mathbb{R}^n$ the reward gradient, $\|\cdot\|_F$ the Frobenius norm, and $\|\cdot\|$ the Euclidean norm. The three subspace-alignment scores are:

- **Reward Controllability Fraction (RCF):** fraction of the reward gradient’s energy in the controllable subspace.

$$\text{RCF} = \frac{\|U_c^{(k)\top} \mathbf{r}\|^2}{\|\mathbf{r}\|^2} \in [0, 1]. \quad (5)$$

- **Observation Controllability Fraction (OCF):** fraction of the decoder’s sensitivity in the controllable subspace.

$$\text{OCF} = \frac{\|C U_c^{(k)}\|_F^2}{\|C\|_F^2} \in [0, 1]. \quad (6)$$

- **Reward Observability Fraction (ROF):** fraction of the reward gradient’s energy in the observable subspace.

$$\text{ROF} = \frac{\|V_o^{(k)\top} \mathbf{r}\|^2}{\|\mathbf{r}\|^2} \in [0, 1]. \quad (7)$$

Each score is recorded for both linearizations: `jac_rcf`, `jac_ocf`, `jac_rof` (fixed) and `jac_dyn_rcf`, `jac_dyn_ocf`, `jac_dyn_rof` (time-varying).

Connection to control theory. Controllability and observability are classical prerequisites for optimal control [7] and carry over directly to MPC and latent-imagination RL, which both roll out the world model through its prior. ROF is the key metric in this regime: it measures the fraction of the reward gradient that lies in the observable subspace, i.e. in the directions that would normally be corrected by the encoder but drift uncorrected during open-loop imagination (see Section 4.7 for the full mechanism).

Curated state sampling. The ROF score is additionally computed twice per linearization: on “good” (return $\geq +100$) and “bad” (return ≤ -100) validation sequences, giving `jac_rof` (good, fixed) and `jac_rof_bad` (bad, fixed), and analogously `jac_dyn_rof` and `jac_dyn_rof_bad` for time-varying. Splitting the classes avoids the seed-dependent batch-composition variance produced by uniform mixing. The headline state-aware metric is the convex combination

$$\text{jac_rof_combined} = \alpha \cdot \text{jac_rof} + (1 - \alpha) \cdot \text{jac_rof_bad}, \quad (8)$$

with $\alpha=0.5$ throughout (a sweep confirms a broad optimum near $\alpha \in [0.3, 0.5]$).

3.4.4 Empirical Sensitivity Metrics

These use finite-difference estimation rather than Jacobians: `emp_C` is the mean pairwise distance between next states produced by different actions (action sensitivity); `emp_O` is the transition response to perturbations in \mathbf{z} (state-perturbation sensitivity); and `emp_L` is the *maximum* over sampled state pairs of $\|f_\theta(\mathbf{s}_1, \mathbf{u}) - f_\theta(\mathbf{s}_2, \mathbf{u})\| / \|\mathbf{s}_1 - \mathbf{s}_2\|$ (the max captures localized blow-ups that the mean would dilute). Together with the two CROF composites defined in Section 3.5, these complete the suite at $5 + 9 + 21 + 3 + 2 = 40$ metrics per checkpoint.

3.5 Composite Reward Observability Fraction (CROF)

`jac_rof_combined` is the strongest single predictor of MPC performance, but at undertrained checkpoints the latent is barely organized and ROF can be artificially small. We therefore introduce the **Composite Reward Observability Fraction (CROF)**, combining ROF with three structural regularizers. We report two variants that share the same four components but use different relative weights:

$$\text{CROF-A} = \widetilde{\text{ROF}} + 1.0 \cdot (1 - \widetilde{k}_c) + 1.0 \cdot (1 - \widetilde{k}_o) + 1.0 \cdot \widetilde{e}_{\text{obs}}, \quad (9)$$

$$\text{CROF-B} = \widetilde{\text{ROF}} + 0.5 \cdot (1 - \widetilde{k}_c) + 0.5 \cdot (1 - \widetilde{k}_o) + 0.5 \cdot \widetilde{e}_{\text{obs}}, \quad (10)$$

where $\widetilde{(\cdot)}$ denotes min-max normalization across all checkpoints, $\text{ROF} = \text{jac_rof_combined}$ from (8), $k_c = \text{jac_ctrl_rank}$, $k_o = \text{jac_obs_rank}$, and $e_{\text{obs}} = \text{ol_obs_avg}$ is the open-loop observation RMSE averaged across all rollout steps. **Lower CROF = better checkpoint**; all four normalized terms are oriented so that smaller is better.

Rationale. ROF is the primary signal; the three regularizers protect against degenerate corners of it: $(1-k_c)$ penalizes low controllability rank, $(1-k_o)$ penalizes low observability rank, and e_{obs} penalizes high open-loop observation RMSE (a sanity check on the dynamics). CROF-A and CROF-B differ only in how heavily these regularizers are weighed against the dominant ROF term; we report both as a transparent ablation rather than picking a single recipe a priori.

4 Experiments

4.1 Environment and Data

We use Gymnasium’s LunarLander-v3 (Section 3.1). The reward decomposes into per-step shaping plus terminal events; we give the explicit formula and analyze its observability in Section 4.8.

We collected 872 human-piloted episodes (180,916 environment steps; 158,685 train + 22,231 validation), split 750/122 train/val (32,038/4,500 valid sequence positions at length 30, stride 5). Two pilots took turns to introduce stylistic diversity, and the mix deliberately covers clean landings, near-misses, and crashes so the world model sees both reward-positive and reward-negative regimes. The dataset is collected once and reused for all model-based training and metric evaluation.

4.2 World Model Training

The RSSM world model (WM) is trained for 500 epochs with learning rate 10^{-4} (AdamW), batch size 64, sequence length 30 at stride 5, KL free-bits floor $\beta_{\text{KL}}=0.5$, and loss weights as in (2). Checkpoints are saved every 5 epochs, yielding 100 for evaluation. All random seeds in this paper (data-loader shuffling, MPC and A2C evaluation episodes, metric sampling, model initialization) are fixed to 12345 so every pair of reported numbers uses identical random draws.

4.3 MPC Evaluation and Metrics

Each of the 100 world model checkpoints (epochs 5, 10, \dots , 500) is evaluated using CEM-MPC (Section 3.2) with deterministic seeding for 20 episodes per checkpoint. We report the mean return across these 20 episodes. CEM parameters: horizon $H=25$, population $N=384$, elites $E=48$, iterations $I=4$, smoothing $\alpha=0.7$, planning discount $\gamma=0.97$.

All metrics from Section 3.4 are computed for each of the 100 checkpoints on the validation set. Per-class ROF metrics additionally use the curated good ($R \geq +100$, 2,713 stride-1 positions) and bad ($R \leq -100$, 1,027 positions) subsets. Jacobian analysis uses $N_J=128$ sampled latent states per checkpoint (per state-class for the curated metrics), each collected after a 5-step posterior warm-up, with a 25-step rollout horizon matching the CEM planning horizon.

4.4 MPC Performance Over Trained World Model Checkpoints

Figure 2 shows CEM-MPC performance across all 100 world model checkpoints. Per-checkpoint mean returns are highly variable (std ≈ 80 –120 across 20 episodes, dominated by LunarLander’s stochastic initial conditions), so we use the 7-point moving-average (MA-7) curve — 140 pooled episodes per smoothed point — as the selection oracle. Three regimes emerge:

- **Early-training / improving** ($\lesssim 200$): the raw curve has occasional spikes (e.g. epoch 60 at +173.5) but the smoothed curve stays below +100 throughout, so these are noisy outliers rather than usable checkpoints.
- **Smoothed peak**: the MA-7 mean peaks at epoch 310 (+153.0) over a broad plateau spanning epochs ~ 260 –320. Selecting the right checkpoint inside this plateau is what CROF is designed to do offline.
- **Late-training collapse** ($\gtrsim 380$): the smoothed return drops sharply (e.g. epoch 405 at -55.4). The collapse is invisible to standard training metrics (validation loss, multi-step RMSE), which keep improving monotonically.

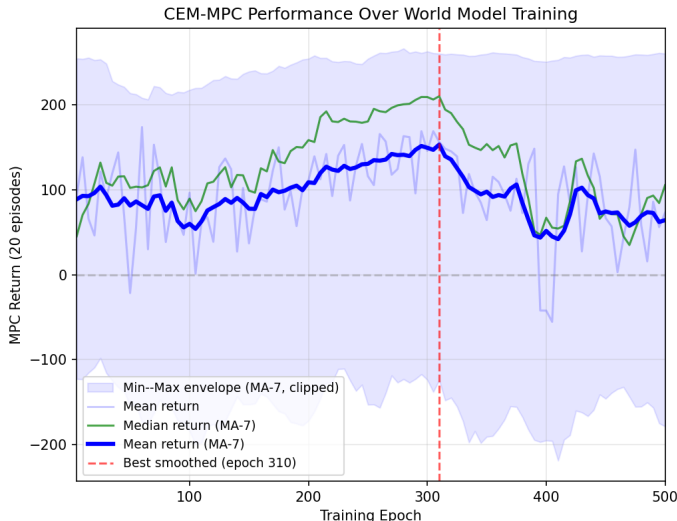


Figure 2: CEM-MPC performance across 500 epochs of world-model training (20 test episodes per checkpoint; 140 pooled per MA-7 point). Bold/faint blue: MA-7-smoothed and raw mean. Green: MA-7-smoothed median. Light band: MA-7 min–max envelope (a few extreme points are clipped). The smoothed mean peaks near epoch 310 and collapses after epoch 380.

4.5 Metric Correlation Analysis

We compute Pearson r , Spearman ρ_s , and quadratic R_q^2 for each metric against the smoothed MPC mean return (7-point moving average). Table 1 consolidates the 40-metric suite from Section 3.4 into

one ranked reference: each row lists what the metric measures and its three correlation scores, with strongly correlated rows in bold. Throughout the paper we use the thresholds *strong*: $|\rho_s| \geq 0.30$, *moderate*: $0.10 \leq |\rho_s| < 0.30$, and *weak*: $|\rho_s| < 0.10$. Figure 6 in Appendix A shows the same Spearman correlations as a bar chart across all 40 metrics, and Figure 7 in the same appendix shows each metric’s full curve over training (only the ROF family traces MPC’s rise–peak–collapse U-shape). ROF based metrics have the strongest correlation with the MPC returns, with Spearman ρ_s in the range $-0.71 \leq \rho_s \leq -0.395$. Some metrics like the validation loss have weak correlation with MPC returns, see Table 1.

4.6 Fixed vs. Time-Varying Jacobian Analysis

Contrary to our initial expectation, the *fixed* linearization is the stronger MPC predictor. The clearest case is ROF: `jac_rof` (fixed, good states) reaches $\rho_s = -0.65$, $R_q^2 = 0.48$ vs. $\rho_s = -0.48$, $R_q^2 = 0.23$ for `jac_dyn_rof`, and the gap on the bad-state subscore widens to $\rho_s = -0.69$ vs. -0.40 (numbers from Table 1). The remaining structural sub-metrics (`spec_radius`, `ctrl/obs_rank`, RCF, OCF) are weakly correlated in both variants and neither wins consistently. We believe the fixed variant wins because chaining $H-1$ Jacobians along an open-loop rollout compounds linearization error while CEM-MPC re-plans each step, so a single Jacobian at the current warm-up-grounded state is closer to the regime CEM actually operates in. We therefore drop time-varying metrics from the CROF formulation; they remain available in the released code.

4.7 ROF as a Predictor of MPC Performance

`jac_rof_combined` is the strongest single predictor in our suite: $\rho_s = -0.71$ ($N=100$, $p \lesssim 10^{-15}$, $R_q^2 = 0.52$; visualized in Figure 3). Both per-class subscores are strong on their own (ρ_s of -0.65 for good states, -0.69 for bad states), so the combined score rests on two largely independent pieces of evidence rather than a single regression artefact.

Analysis. ROF measures how much of the reward gradient lies in the observable subspace. The posterior anchors that subspace during training using real observations, but CEM-MPC and latent-imagination A2C roll the prior in imagination for $H=25$ steps with no encoder corrections, so the observable directions drift uncorrected. A reward head that reads predominantly from those directions (high ROF) therefore degrades along the rollout, while a head that reads from the complementary subspace (low ROF) remains accurate. Section 4.8 confirms that LunarLander’s reward sits exactly in this regime: $\sim 71\%$ of per-step reward variance is unrecoverable from (o_t, a_t) alone, so a well-trained world model must encode that part outside the observation-decoder column space.

4.8 Reward Predictability from Observations

LunarLander’s per-step reward, taken from the Gymnasium reference implementation,¹ has the form

$$r_t = \underbrace{\phi(o_{t+1}) - \phi(o_t)}_{\text{PBRs shaping}} - c_{\text{main}} \mathbb{1}[a_t = \text{main}] - c_{\text{side}} \mathbb{1}[a_t \in \{\text{L}, \text{R}\}] + r_t^{\text{term}}, \quad (11)$$

with shaping potential $\phi(o) = -100(\|p\| + \|v\|) - 100|\theta| + 10(\text{leg}_1 + \text{leg}_2)$ defined on the visible state, $(c_{\text{main}}, c_{\text{side}}) = (0.30, 0.03)$, and $r_t^{\text{term}} \in \{-100, +100, 0\}$ awarded only at episode end and gated by

¹https://github.com/Farama-Foundation/Gymnasium/blob/main/gymnasium/envs/box2d/lunar_lander.py

Metric	What it measures	Pearson r	Spearman ρ_s	R_q^2
<i>Strong predictors ($\rho_s \geq 0.30$, bold)</i>				
<code>jac_rof_combined</code>	$0.5 \cdot \text{jac_rof} + 0.5 \cdot \text{jac_rof_bad}$, state-aware ROF	-0.683	-0.710	0.520
<code>jac_rof_bad</code>	Fixed-Jacobian ROF on bad (low-return) sequences	-0.656	-0.692	0.434
<code>jac_rof</code>	Fixed-Jacobian ROF on good (high-return) sequences	-0.558	-0.648	0.479
CROF-B	Composite: ROF + $0.5 \times$ rank/OL-err regularizers	-0.495	-0.568	0.421
<code>jac_dyn_rof</code>	Time-varying ROF on good sequences	-0.467	-0.477	0.229
CROF-A	Composite: ROF + $1.0 \times$ rank/OL-err regularizers	-0.375	-0.443	0.243
<code>jac_dyn_rof_bad</code>	Time-varying ROF on bad sequences	-0.277	-0.395	0.182
<code>ol_rew_end</code>	Open-loop reward RMSE at horizon step 25	+0.272	+0.301	0.101
<code>val_kl</code>	KL component of validation loss	+0.206	+0.300	0.064
<i>Moderate predictors ($0.10 \leq \rho_s < 0.30$)</i>				
<code>jac_dyn_obs_cond</code>	Condition number of time-varying observability matrix	+0.243	+0.273	0.074
<code>val_recon</code>	Reconstruction component of validation loss	-0.082	-0.184	0.018
<code>jac_spec_radius</code>	Spectral radius of fixed-Jacobian dynamics	-0.157	-0.172	0.055
<code>emp_L</code>	Max-Lipschitz of f_θ over state pairs	+0.327	+0.154	0.110
<code>emp_0</code>	State-perturbation sensitivity (finite-difference)	+0.104	+0.130	0.051
<code>ol_rew_start</code>	Open-loop reward RMSE at horizon step 1	-0.156	-0.128	0.086
<i>Representative weak / near-zero baselines ($\rho_s < 0.10$)</i>				
<code>val_loss</code>	Total weighted validation loss	+0.029	+0.090	0.015
<code>post_obs_rmse</code>	One-step posterior observation RMSE	-0.084	+0.012	0.010
<code>post_rew_rmse</code>	One-step posterior reward RMSE	+0.028	+0.085	0.018
<code>ol_obs_avg</code>	Open-loop observation RMSE averaged over horizon	-0.087	+0.017	0.011
<code>ol_cumrew_err</code>	Open-loop cumulative-reward RMSE	+0.002	+0.107	0.062
<code>jac_ctrl_rank</code>	Effective controllability rank (fixed Jacobian)	+0.113	+0.015	0.013
<code>emp_C</code>	Action sensitivity (finite-difference)	+0.069	-0.093	0.029

Table 1: Representative metrics from the 40-metric suite (Section 3.4), ranked by Spearman $|\rho_s|$ against smoothed MPC mean return (MA-7, $N=100$ checkpoints). To save space we only list the most informative metrics by correlation and a few additional metrics included by relevance (standard training/prediction baselines, control-theoretic ranks, finite-difference sensitivities); the remaining ~ 18 metrics not listed all sit inside the weak band. Top block (bold): the 9 strongly correlated metrics — the ROF/CROF family dominates, joined by `ol_rew_end` and `val_kl`. Middle block: 6 moderately correlated metrics. Bottom block: 7 near-zero baselines, where all standard training and one-step-prediction metrics fall. Equations: `jac_rof_combined` (8), ROF (7), CROF-A/B (9)/(10).

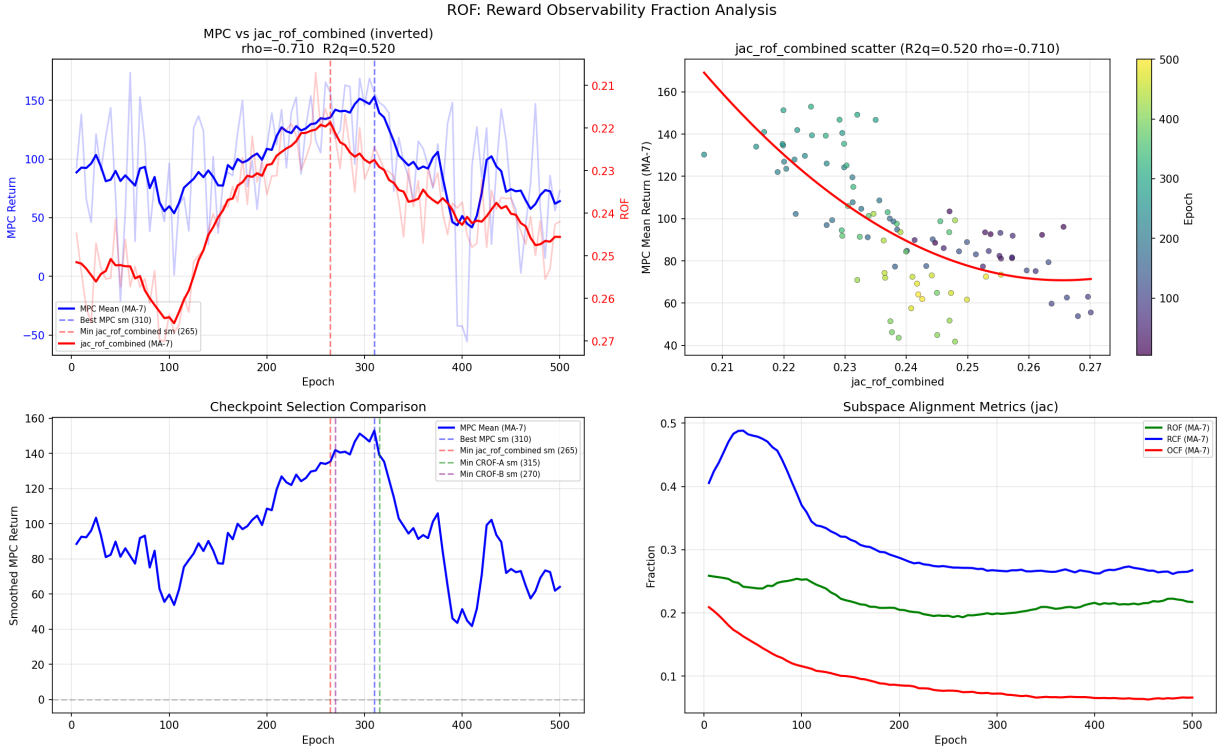


Figure 3: ROF analysis. Top-left: smoothed MPC return (blue) vs. inverted `jac_rof_combined` (red), with vertical lines at the smoothed MPC peak (epoch 310) and the smoothed `jac_rof_combined` minimum (epoch 265). Top-right: per-checkpoint scatter with quadratic fit, exhibiting the characteristic U-shape (smoothed Spearman $\rho_s = -0.71$, $R^2_q = 0.52$). Bottom-left: checkpoint selection comparison — the MA-7-smoothed `jac_rof_combined` minimum and the MA-7-smoothed CROF-A and CROF-B picks all sit inside or adjacent to the high-MPC plateau (raw minima in Table 2). Bottom-right: subspace alignment metrics (RCF, OCF, ROF) vs. epoch.

Box2D-internal flags (`game_over`, `lander.awake`) absent from o_t . Two pieces of this expression—the $\phi(o_{t+1})$ term and r_t^{term} —are structurally not recoverable from (o_t, a_t) , which is what we measure below.

To measure how much of r_t is recoverable from observations alone, we trained MLP regressors (two hidden layers of 256 units, ReLU, AdamW, MSE loss) on the same dataset, in four input configurations and computed R^2 score for each that measures the percentage of the data the model can explain from its input. We got the following results: R^2 : 0.290 for (o_t, a_t) input alone, 0.670 when terminal events are filtered out (steps where `done=1` which account $<1\%$ of data), 0.595 when o_{t+1} is added, and **0.971** when both terminals are filtered and o_{t+1} is added.

Reading the decomposition: (o_t, a_t) alone leaves $\sim 71\%$ of per-step reward variance unexplainable; adding o_{t+1} and filtering terminals recovers more reward. A sequence-model latent can track the missing context from the trajectory history, so the reward head must read from directions outside the observation-decoder column space. ROF measures the fraction of the reward gradient that lies *inside* that column space, so lower ROF marks the checkpoints where the reward head has moved its computation to where it belongs.

Reacher: a Markovian-reward contrast. As a sanity check on the structural argument, we re-ran the same MLP regression and the same Jacobian-based diagnostic suite on a Gymnasium Reacher world model trained with an identical RSSM setup. Predicting r_t from (o_t, a_t) alone gives MLP validation $R^2 = 0.9998$: Reacher’s reward is fully Markovian in the observation–action pair. Correspondingly, `jac_rof_combined` is essentially uninformative about closed-loop performance — Spearman $\rho_s = +0.143$ against smoothed MPC return ($R_q^2 = 0.265$), opposite in sign to LunarLander’s -0.71 , and MPC return rises nearly monotonically over training rather than tracing the LunarLander U-shape (Figure 4). On this task there is no checkpoint-selection problem for ROF to solve: standard one-step prediction metrics work fine.

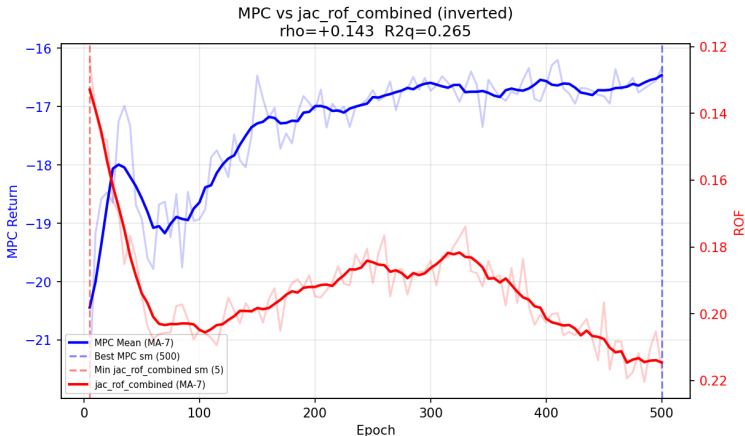


Figure 4: Reacher contrast. Smoothed MPC return (blue) and inverted `jac_rof_combined` (red) over training on a Gymnasium Reacher world model trained with the identical RSSM setup. Both curves rise nearly monotonically; there is no U-shape and no late-training collapse, and the rank correlation between the two ($\rho_s = +0.143$, $R_q^2 = 0.265$) is weak and of the opposite sign to LunarLander.

When ROF carries signal. The structural condition for ROF to be informative appears to be that the reward is not Markovian in (o_t, a_t) , so a well-trained world model has to encode

reward-relevant quantities in latent directions outside the observation-decoder column space. This class includes tasks with PBRS shaping [10], tasks whose terminal or sparse rewards depend on hidden simulator state, and partially observed control tasks more generally. LunarLander is a representative example of such setups. We therefore present CROF as a metric targeting this practically common structural condition rather than as a domain-agnostic rule.

4.9 Checkpoint Selection via CROF and Structural Insights

Table 2 compares checkpoint-selection criteria: the smoothed-MPC oracle, raw and smoothed-min picks of the structural metrics, and representative weak baselines; Figure 5 plots smoothed CROF-A and CROF-B against MPC return with the same picks marked.

Selection rule	Epoch selected	MPC return
<i>Oracle baseline</i>		
Best smoothed MPC (oracle, MA-7)	310	+153.0
<i>Structural / proposed metrics</i>		
Min CROF-A (raw)	280	+162.8
Min CROF-A (smoothed MA-7)	315	+148.1
Min CROF-B (raw)	280	+162.8
Min CROF-B (smoothed MA-7)	270	+117.5
Min jac_rof_combined (raw)	250	+115.8
Min jac_rof_combined (smoothed MA-7)	265	+156.5
<i>Standard / weak baselines</i>		
Min val_loss	470	+79.3
Min post_rew_rmse	470	+79.3
Min ol_obs_end	495	+55.9
Min ol_cumrew_err	460	+2.9
Max emp C	485	+15.6
Max jac_ctrl_rank	445	+115.8

Table 2: Checkpoint selection comparison. The smoothed (MA-7) MPC oracle peaks at epoch 310 with a plateau over epochs 260–320; both CROF variants’ raw-minimum picks (epoch 280) land inside it. The pure-ROF baseline (`jac_rof_combined`) picks epoch 250 raw / 265 smoothed — only the smoothed pick is in the plateau, motivating the CROF auxiliary terms. All standard criteria pick deeply overfit checkpoints (epoch ≥ 460) with MPC returns of +3 to +79.

ROF and CROF are also the only metrics whose informativeness peaks in the regime one would actually select from: a phase-wise breakdown shows `jac_rof_combined` reaches Pearson $r=-0.65$ in mid-training (epochs 100–300) versus -0.20 early and -0.32 late.

Two observations from the Jacobian analysis tell the broader story. First, controllability is low-dimensional: $k_c \approx 33-47$ out of $n=272$ latent dimensions ($\sim 12-17\%$), with the GRU’s gating preserving historical context in the rest. Second, overfitting is *structural*: multi-step prediction RMSE keeps improving long after the rewards/observations/controllable subspaces have drifted out of alignment, which is what hurts closed-loop MPC.

4.10 Model-Based Actor-Critic Policy Training Performance

To test whether the CROF-driven checkpoint selection (Section 4.9) translates into competitive downstream model-based A2C policies, we train one A2C agent per world-model (WM) checkpoint

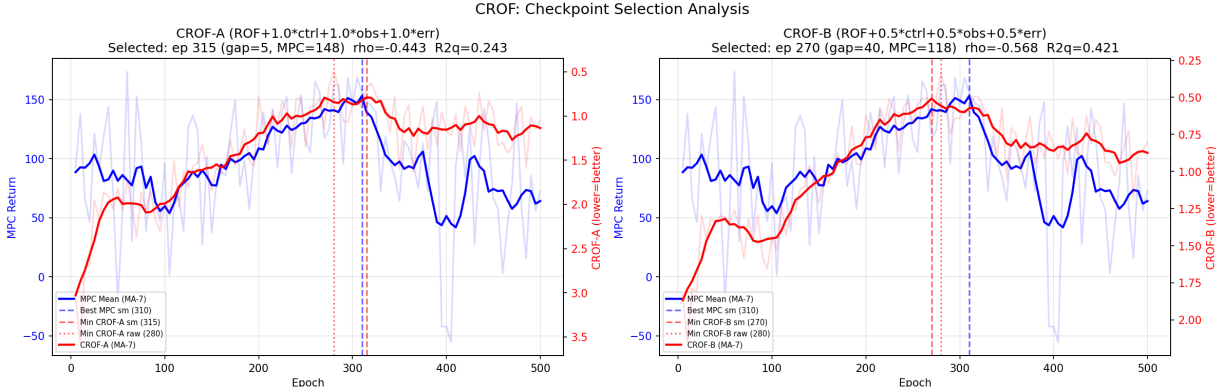


Figure 5: CROF composite score over training. Left: smoothed MPC return (blue) vs. smoothed CROF-A (red, lower-is-better axis inverted). Right: same for CROF-B. Vertical lines mark the smoothed MPC oracle (blue dashed, epoch 310), the MA-7-smoothed CROF minimum (red dashed: CROF-A at 315, CROF-B at 270), and the raw CROF minimum (red dotted: 280 for both variants); see Table 2.

over a *purposive* sample of nine WMs that includes the CROF-A/B and pure-ROF picks alongside oracle, plateau, pre-plateau, and three early-training references (per-WM selection rules in Table 3; WM 60 is the raw-MPC outlier from Section 4.4). A uniform sweep over all 100 WMs would be prohibitive. All nine runs share the hyperparameters of Section 3.3 (1000 epochs, a checkpoint every 50 epochs, seed 12345), and every saved actor is evaluated on 100 deterministic episodes in the real environment (seed sequence $12345+k$, $k = 0, \dots, 99$, max 600 steps) reporting mean, worst-case, catastrophic failures (return < -100), and perfect landings (return $\geq +200$, the LunarLander “solved” threshold).

Table 3 reports, per WM checkpoint, the A2C checkpoint with the highest mean return (“best-by-mean”, BBM) and the checkpoint with the highest worst-case return (“safest-by-worst”, SBW); SBW is the more practically useful pick for deployment, where worst-case behavior matters.

WM Selection rule	Best-by-mean A2C checkpoint					Safest-by-worst A2C checkpoint					
	Ep.	Mean	Worst	Catas	Perfect	Ep.	Mean	Worst	Catas	Perfect	#safe
50 early training	550	+178.3	-120.8	5	64	900	+141.3	-74.7	0	47	1/20
60 raw-MPC outlier	500	+206.3	-157.3	5	79	600	+182.1	-154.7	8	73	0/20
100 early training	800	+223.3	-108.0	1	85	200	+65.0	-80.2	0	25	3/20
200 pre-plateau reference	1000	+191.4	-184.2	3	70	300	+149.1	-111.3	1	43	0/20
250 min jac_rof_combined (raw)	300	+141.0	-161.2	1	26	200	+127.3	-104.8	1	28	0/20
280 min CROF-A, CROF-B (raw)	800	+217.5	-178.9	2	79	300	+191.3	-39.6	0	71	2/20
300 plateau midpoint	850	+205.9	-95.5	0	74	600	+138.3	-63.1	0	49	7/20
310 smoothed-MPC oracle	1000	+209.6	-131.0	2	75	400	+196.0	-40.4	0	52	3/20
315 min CROF-A (sm. MA-7)	800	+178.0	-203.5	1	63	700	+133.1	-72.1	0	47	1/20

Table 3: A2C training outcomes across purposively sampled world-model checkpoints, 100 deterministic episodes per A2C checkpoint (bold rows mark CROF metric-driven picks). **Ep.** is the AC training epoch of the reported checkpoint; **mean/worst** are mean and worst-case return; **catas** counts episodes with return < -100 , **perfect** counts $\geq +200$; **#safe** is the number of A2C checkpoints (out of 20) with 0 catastrophic episodes. The *best-by-mean* (BBM) and *safest-by-worst* (SBW) blocks report, respectively, the A2C checkpoint with the highest mean and the checkpoint with the highest worst-case return.

Analysis. A deployable WM is one whose BBM and SBW checkpoints both report a high mean. By that joint criterion CROF’s raw pick WM 280 wins: BBM +217.5 and SBW +191.3 with a ~ 26 -point peak-to-safe gap, found offline with no environment evaluation. The smoothed-MPC oracle (WM 310) is comparable but requires the full MPC sweep to identify. WM 100 is the trap that the BBM column alone hides: highest BBM (+223.3), but its SBW checkpoint collapses to +65.0 — a ~ 158 -point peak-to-safe gap. WM 250 (raw min of `jac_rof_combined` alone) is the weakest deployable WM, showing that CROF’s auxiliary terms are doing real work: they nudge the selection out of the local-ROF dip at WM 250 into the structurally good region around WM 280.

4.11 Model-Free Actor-Critic Policy

As a baseline, we train a model-free A2C agent (MF-AC) that interacts directly with the real environment. Actor and critic are 3-layer MLPs of width 256 over the raw observation; training runs for 1000 epochs at 50 episodes per epoch (50,000 total episodes, ≈ 18.4 M transitions, mean episode length ≈ 368), with learning rate 3×10^{-4} , $\gamma=0.99$, $\lambda=0.95$, entropy decayed from 0.2 to 0.01.

MF-AC is evaluated with the same 100-episode protocol used for WM-AC, but with LunarLander’s standard 1000-step horizon (WM-AC and MPC use a 600-step cap matching MPC’s per-step inference budget) to give the baseline its strongest evaluation. MF-AC peaks at AC epoch 760 with mean return +**193.04** (54/100 perfect, **0/100** catastrophic, worst -35.55) and forms a reliable plateau over epochs ~ 610 – 910 in the +170 to +195 band. The head-to-head against WM-AC is reported in Table 4: MF-AC has the tightest worst-case, while WM-AC has higher mean and more perfect landings at a fraction of the data cost.

4.12 Data Efficiency Comparison

We measure training data efficiency cost for CEM-MPC, WM-AC, and MF-AC. We use real environment steps so they are compared on the same axis. All model-based methods share the same offline dataset (180,916 steps over 872 episodes); MF-AC’s cost is the cumulative transition count up to its best epoch 760. Table 4 summarizes the result.

Method	Env. steps	Mean	Worst	Perfect	Catast.	Data vs. MF-AC
MPC (smoothed best, WM 310)	180,916	+166.60	-138.52	64/100	3/100	65.3 × fewer
WM-AC (CROF raw, WM 280, A2C ep 800)	180,916	+217.48	-178.86	79/100	2/100	65.3 × fewer
WM-AC (CROF-A smooth, WM 315, A2C ep 800)	180,916	+178.01	-203.47	63/100	1/100	65.3 × fewer
MF-AC (peak @ ep 760)	11,820,726	+193.04	-35.55	54/100	0/100	1× (baseline)

Table 4: Real environment-step cost vs. deterministic-policy mean return (100 episodes per checkpoint). MPC and WM-AC use a 600-step cap matching MPC’s inference budget; MF-AC uses the standard 1000-step LunarLander-v3 horizon under which it was trained. All model-based methods reuse the same 872-episode offline dataset (180,916 env. steps). **Perfect** = return $\geq +200$ (“solved”); **Catast.** = return < -100 . Each WM-AC row reports the BBM A2C checkpoint inside the corresponding CROF-selected WM (Table 3). The CROF raw pick (**WM 280**) is the strongest model-based result, beating MF-AC’s peak by ~ 24.5 points at ~ 65 × fewer real environment interactions; MF-AC is the only method with 0/100 catastrophic but at two orders of magnitude higher data cost.

Analysis. The CROF raw WM-AC pick (WM 280, identified offline) reaches peak mean +**217.48** and requires ~ 65.3 × fewer real-environment interactions than MF-AC; CEM-MPC on the same

WM family already reaches +**166.6** at $n=100$ with no policy training. At inference time, the trained A2C policy is $\sim 1000\times$ cheaper to execute than CEM-MPC, which runs 4 iterations of 384 rollouts $\times 25$ steps at every real timestep. This confirms substantially higher training-data efficiency for the world-model-based methods.

5 Conclusion

We presented a study of validation-time metrics for predicting the closed-loop performance of a learned latent world model, using LunarLander-v3 as the testbed and the *Composite Reward Observability Fraction* (CROF) as a candidate single-number score for offline checkpoint selection. On this task CROF tracks both CEM-MPC and model-based A2C performance, while standard criteria (validation loss, multi-step RMSE, empirical sensitivities) instead pick deeply overfit checkpoints where MPC has poor closed-loop performance.

The CROF raw pick (WM 280) yields a model-based A2C with peak mean return +**217.5** (79/100 perfect landings) — ~ 24.5 points above the model-free A2C baseline (+193.0) at $\sim 65\times$ fewer real-environment interactions. The smoothed-MPC oracle (WM 310, identifiable only via the full MPC sweep) yields a comparable WM-AC peak of +209.6, so on this task CROF matches an oracle pick at zero real-environment-selection cost.

Scope and limitations. All quantitative claims here are on a single environment (LunarLander-v3). The mechanistic argument for ROF leans on the specific structure of LunarLander’s reward (per-step shaping plus terminal events gated by simulator-internal flags), so we expect ROF to carry less signal on tasks whose reward is fully Markovian in (o_t, a_t) — a Reacher control we report in Section 4.8 confirms this directionally (MLP $R^2 = 0.9998$, ROF Spearman $\rho_s = +0.143$). We therefore present CROF as a metric that targets a specific, but practically common, structural condition where rewards are non-Markovian or shaped rather than as a domain-agnostic metric.

Future work. Natural extensions include cross-environment validation (continuous actions, higher-dimensional observations, varied reward structures), using a ROF-like term as an auxiliary training regularizer, and developing an analogous offline metric for A2C-policy checkpoint selection — an obvious gap in the current pipeline, where the final actor checkpoint still requires real-environment evaluation.

References

- [1] Rishabh Agarwal, Marlos C. Machado, Pablo Samuel Castro, and Marc G. Bellemare. Contrastive behavioral similarity embeddings for generalization in reinforcement learning. In *International Conference on Learning Representations (ICLR)*, 2021.
- [2] Kurtland Chua, Roberto Calandra, Rowan McAllister, and Sergey Levine. Deep reinforcement learning in a handful of trials using probabilistic dynamics models. In *Advances in Neural Information Processing Systems (NeurIPS)*, volume 31, 2018.
- [3] Carles Gelada, Saurabh Kumar, Jacob Buckman, Ofir Nachum, and Marc G. Bellemare. Deep-MDP: Learning continuous latent space models for representation learning. In *International Conference on Machine Learning (ICML)*, pages 2170–2179. PMLR, 2019.

- [4] Danijar Hafner, Timothy Lillicrap, Jimmy Ba, and Mohammad Norouzi. Dream to control: Learning behaviors by latent imagination. In *International Conference on Learning Representations (ICLR)*, 2020.
- [5] Danijar Hafner, Timothy Lillicrap, Ian Fischer, Ruben Villegas, David Ha, Honglak Lee, and James Davidson. Learning latent dynamics for planning from pixels. In *International Conference on Machine Learning (ICML)*, pages 2555–2565. PMLR, 2019.
- [6] Danijar Hafner, Jurgis Pasukonis, Jimmy Ba, and Timothy Lillicrap. Mastering diverse domains through world models. *arXiv preprint arXiv:2301.04104*, 2023.
- [7] Rudolf E. Kalman. Mathematical description of linear dynamical systems. *Journal of the Society for Industrial and Applied Mathematics, Series A: Control*, 1(2):152–192, 1963.
- [8] Nathan Lambert, Brandon Amos, Omry Yadan, and Roberto Calandra. Objective mismatch in model-based reinforcement learning. In *Proceedings of the 2nd Conference on Learning for Dynamics and Control (L4DC)*, pages 761–770. PMLR, 2020.
- [9] Bruce C. Moore. Principal component analysis in linear systems: Controllability, observability, and model reduction. *IEEE Transactions on Automatic Control*, 26(1):17–32, 1981.
- [10] Andrew Y. Ng, Daishi Harada, and Stuart Russell. Policy invariance under reward transformations: Theory and application to reward shaping. In *International Conference on Machine Learning (ICML)*, pages 278–287, 1999.
- [11] Reuven Y. Rubinstein. The cross-entropy method for combinatorial and continuous optimization. *Methodology and Computing in Applied Probability*, 1(2):127–190, 1999.
- [12] John Schulman, Philipp Moritz, Sergey Levine, Michael I. Jordan, and Pieter Abbeel. High-dimensional continuous control using generalized advantage estimation. *arXiv preprint arXiv:1506.02438*, 2015.
- [13] David Sussillo and Omri Barak. Opening the black box: Low-dimensional dynamics in high-dimensional recurrent neural networks. *Neural Computation*, 25(3):626–649, 2013.
- [14] Marvin Zhang, Sharad Vikram, Laura Smith, Pieter Abbeel, Matthew J. Johnson, and Sergey Levine. SOLAR: Deep structured representations for model-based reinforcement learning. In *International Conference on Machine Learning (ICML)*, pages 7444–7453. PMLR, 2019.

A Supplementary Figures

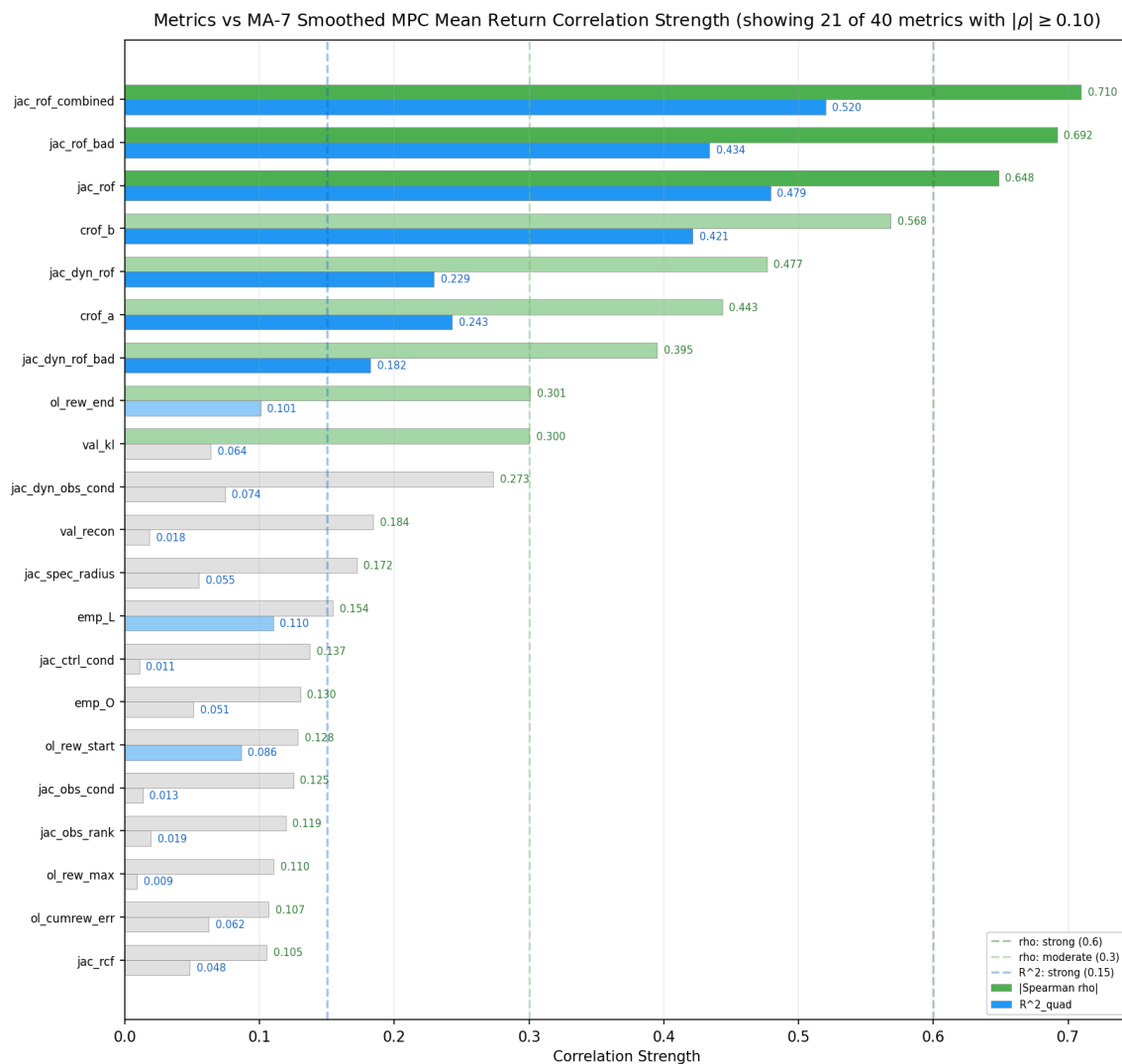


Figure 6: Per-metric correlations with smoothed (MA-7) MPC mean return for all 40 metrics in the suite of Section 3.4. Bars show Spearman ρ_s ; colours mark the strong ($|\rho_s| \geq 0.30$), moderate ($0.10 \leq |\rho_s| < 0.30$), and weak ($|\rho_s| < 0.10$) bands used throughout the paper. The ROF/CROF family dominates the strong-correlation block, while all standard training and one-step-prediction metrics (`val_loss`, `val_recon`, `post_*_rmse`, etc.) sit in the weak band. Numerical values for the most informative subset are listed in Table 1.

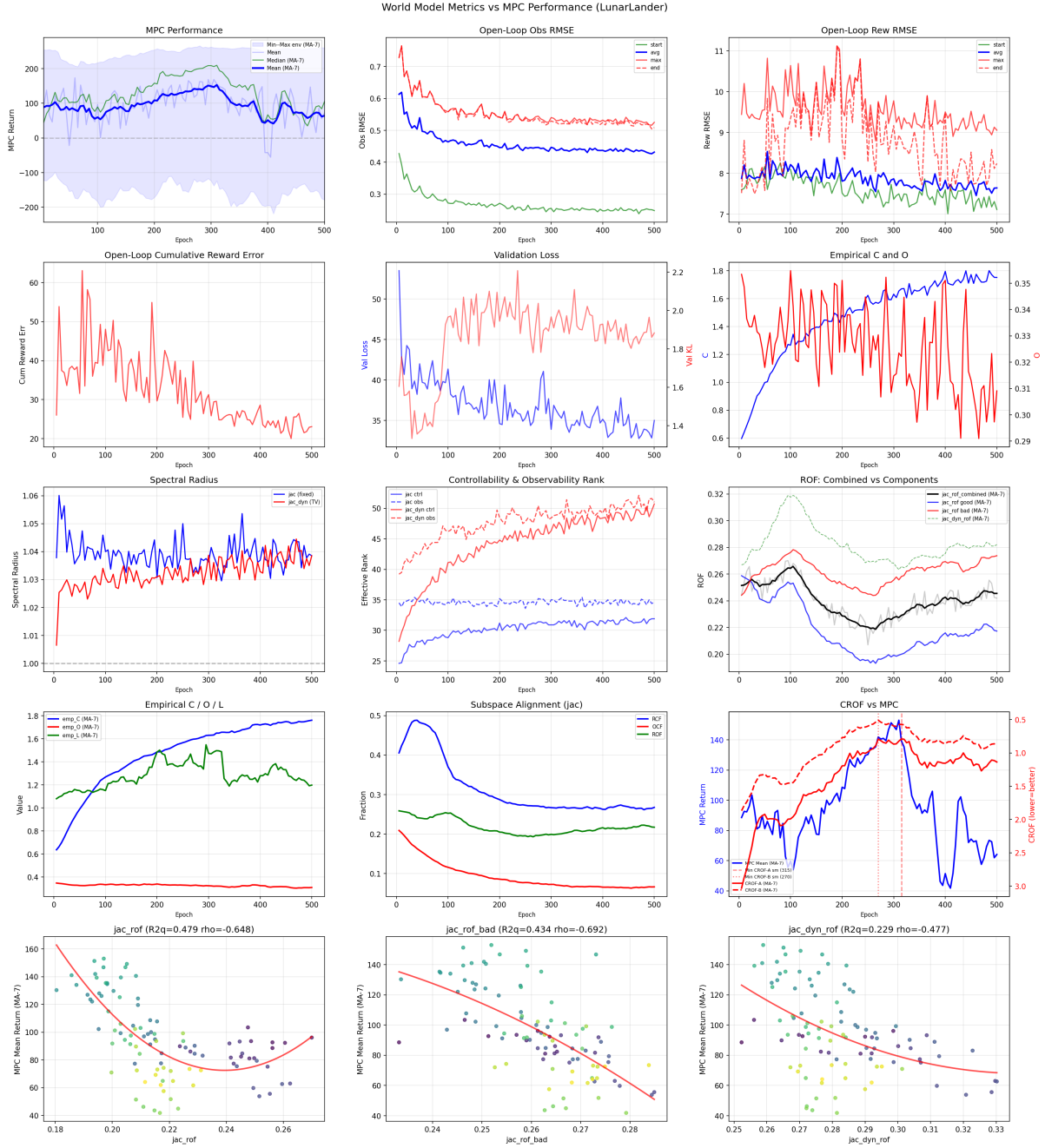


Figure 7: Metrics vs. MPC dashboard. Standard metrics (validation losses, open-loop RMSEs, empirical sensitivities, Jacobian spectral radius and ranks) are monotonic or flat through the late-training collapse; only the ROF family (third-row right panel) traces MPC’s rise–peak–collapse U-shape. Bottom row: scatter of the three core ROF sub-metrics against MA-7 MPC return with quadratic fits.